Proceedings of the 2004 ASME Heat Transfer/Fluids Engineering Summer Conference
July 11-15, 2004, Charlotte, NC, USA

DRAFT **HT-FED2004-56169**

TIME AND SPACE RESOLVED WALL TEMPERATURE MEASUREMENTS DURING NUCLEATE BOILING WITH CONSTANT HEAT FLUX BOUNDARY CONDITIONS

Jerry G. Myers (1), Sam W. Hussey (1), and Glenda F. Yee (1), Vamsee K. Yerramilli (2), and Jungho Kim (2)

(1) National Aeronautics and Space Administration
Glenn Research Center
Microgravity Science Division
Brookpark, Ohio

(2) Department of Mechanical Engineering
University of Maryland
College Park, Maryland

ABSTRACT

The lack of temporally and spatially resolved measurements under nucleate bubbles has complicated efforts to fully explain pool-boiling phenomena. The objective of this current work is to acquire time and space resolved temperature distributions under nucleate bubbles on a constant heat flux surface. This was performed using a microheater array with 100 μm resolution that allowed effectively simultaneous measurements of surface temperature while supplying a constant dissipative heat flux. This data is then correlated with high speed (> 1000Hz) visual recordings of the bubble growth and departure from the heater surface acquired from below and from the side of the heater. The data indicate that a significant source of energy during bubble nucleation and initial growth is the superheated layer around the bubble. Bubble coalescence was not observed to decrease surface temperature as significantly as bubble departure from the surface. Since bubble departure is typically followed by a sharp increase in the heater surface temperature, it is surmised that the departing bubble effectively removes the superheated layer, allowing a higher local heat transfer rate with the bulk fluid through transient conduction/micro-convection during rewetting.

INTRODUCTION

Investigations into single bubble pool boiling phenomena are often complicated by the difficulties in obtaining time and space resolved information in the bubble region since the heaters and diagnostics used to measure heat transfer data are often on the order of, or larger than, the bubble characteristic length or region of influence. This has contributed to the development of many different and sometimes contradictory models of pool boiling phenomena and dominant heat transfer mechanisms.

Mikic and Rosenhow [1] proposed a transient conduction model in which the departing bubble removed a portion of the superheated liquid layer twice the bubble departure diameter. Cold bulk liquid was assumed to rewet the surface immediately after bubble departure and transient conduction into this liquid occurred until nucleation of the next bubble. Cooper and Lloyd [2] measured wall temperature variations under bubbles using micro-thermocouples, and proposed that bubble heat transfer occurred through the formation and evaporation of a thin liquid layer (the microlayer) between the growing bubble and the wall. Stephan and Hammer [3] proposed that the heat transfer occurred primarily at the three-phase contact line where the liquid-vapor interface approaches the wall according to the mechanism proposed by Wayner et al. [4].

Yaddanapudi and Kim [5] measured local heat transfer underneath single bubbles nucleating periodically from a single site for saturated FC-72 at 1 atm (T_{sat}=56.7 °C) and with the wall held at a constant wall temperature of 79.2 °C using a microheater array with individual heaters 270 μm in size. The bubble departure diameter was about 370 μm, only slightly larger than a single heater. Their results indicated that bubble growth occurred primarily due to energy gained from the superheated liquid layer. Bubble departure resulted in rewetting of the wall by colder liquid, and heat transfer through transient conduction and/or microconvection, consistent with the model of Mikic and Rosenhow [1].

Demiray and Kim [6] presented local heat transfer data underneath bubbles nucleating from a single site for single and vertically merging bubbles under conditions similar to Yaddanapuddi and Kim [5], but using an array with heaters 100 μm in size. The surface temperature of the heater array and the bulk fluid temperature during the experiment were 76 °C and 52 °C, respectively. Bubbles that nucleated at this site alternated between two modes: single bubble mode and

multiple bubble mode. In the single bubble mode, discrete bubbles departed from the heater array with a waiting time between the departure of one bubble and nucleation of the following bubble. In the multiple bubble mode, bubble nucleation was observed immediately after the previous bubble departed. The departing bubble pulled the growing bubble off the surface prematurely and the bubbles merged vertically forming small vapor columns. The data indicated that the area influenced by a single bubble departing the surface was approximately half the departure diameter. Microlayer evaporation was observed to contribute a significant, but not dominant, fraction of the wall heat transfer in the single bubble mode where a long waiting time preceeded bubble nucleation. Microlayer evaporation was insignificant in the multiple bubble mode, and heat transfer occurred mainly through transient conduction and/or microconvection during liquid rewetting as the bubble departed the surface.

This study seeks to expand on the previous work by making time and space resolved measurements under bubbles nucleating on a microheater array operated under constant heat flux conditions. Wall temperature distributions were measured throughout the bubble nucleation and departure cycle using an array with microheaters 100 μm in size, and were synchronized with high-speed videos. A description of the experimental setup, the results, and implications for modeling boiling heat transfer are presented.

EXPERIMENTAL APPARATUS

Heater Array. The heater array in this experiment is similar to those used by Demiray and Kim [6]. The array consisted of 96 platinum resistance heaters microfabricated in a 10x10 configuration on a 500 μm thick quartz wafer/substrate (Figure 1). After cleaning the as-received wafers, a 30 nm thick Ti adhesion layer was deposited onto the quartz followed by a 400 nm Pt layer. Standard photolithography was used to pattern the photoresist, and an ion mill was used to form the individual heaters followed by a plasma ash. Gold power leads 1 μm thick were then deposited to allow connections to be made to the heaters.

Each array element was square with a nominal area of $0.01mm^2$ and consisted of 2 μm wide Pt lines spaced 2 μm apart. Each heater exhibited a nominal resistance of 6 kΩ and a temperature coefficient of resistance of ~10 Ω $^{\circ}C^{-1}$. Gold lines that supply power to the heaters were routed between the heaters.

Control Circuit. Each heater was supplied with constant power by individual circuits consisting of a Wheatstone bridge and amplifier as shown on Figure 2. R1 was close to Rh in value, and was tailored for each circuit so that all heaters dissipated similar heat fluxes for a given V_{top} (voltage supplied to the bridge, See Figure 2). The ratio of R2/R3 was similar to Rh/R1 at room temperature to minimize the offset voltage entering the amplifier. The analog output from each of the circuits was linearly proportional to V_{heater}. The heater power could be changed using V_{top}, and the heater current could be computed from

$$i_{heater} = \frac{V_{top} - V_{heater}}{R1}$$

The power dissipated by a heater is $q = i_{heater} V_{heater}$. Although Rh increases as the heater temperature rises, the voltage across the heater V_{heater} also increases, resulting in a power dissipation that is essentially constant over the range of expected operating temperatures.

Twenty-four circuits were constructed on a single card, requiring 4 cards to control the array. All 4 cards are connected to a custom designed multiplexer board that controlled the V_{top} and acted as a router between the individual circuits and the computer/DAQ system.

Heater Calibration. Calibration of the heater array was performed using a two-step process. Initially the variation of heater resistance with temperature was determined by placing the array in an oven held to within 0.1 °C of the set temperature and measuring the resistance of each heater over a range of temperatures from 40 °C to 100 °C. Two thermocouple attached to the underside of the heater assembly were used to ensure stability of the temperature environment. Figure 3 illustrates the results of this calibration step for four selected heaters on the array.

The second step in the calibration involved calibrating the measured output voltage from each heater circuit (relative to the applied power) with the resistance of the heater. In this calibration step, the control boards and multiplexer were connected to banks of known resistors (nominally 6, 7 and 8 kΩ). The output voltages and data acquisition readings of each heater circuit were then measured at each resistance level. Since an amplifier's output voltage was directly correlated to the resistance of a heater, this two-step process provided measurements of heater temperature with an expected uncertainty less than 1 °C.

Boiling Rig. The boiling rig was custom designed and built at the NASA Glenn Research Center (illustrated in Figure 4) to handle FC-72, which is used as the working fluid in this experiment. The boiling chamber was a rectangular 9x9x14 cm aluminum chamber with a bellows pressure control system. The chamber incorporated three 5 cm diameter view ports to allow optical access to the heater array. External surface mounted heaters (Thermofoil, Minco Products, Inc.) were attached to the chamber and covered by foam insulation to control the bulk fluid temperature. Fluid access ports were placed on one side of the chamber to allow mixing with an external pump if stratification was detected. Bulk fluid temperature was measured by two T-type thermocouples placed at different heights in the chamber. Chamber pressure was measured by an absolute pressure transducer (0-345 kPa, +/- 0.4 kPa) through an access port on one side of the chamber.

Data Acquisition and High Speed Video. A single data acquisition card (PCI-DIO96, Measurement Computing Corp.)

capable of scanning 96 channels at 200kHz was installed in a Compaq Deskpro (Pentium III, 667MHz) computer and connected directly to the custom multiplexer board. Custom software, written in C, was created to control the experiment. The combined system was capable of obtaining time resolved temperature data from each heater at a rate of 1130 Hz for a set period of time (usually less than 20 seconds).

Temperature acquisition was synchronized with high-speed video acquisition. Because of the semi-transparent nature of the heater and substrate, it was possible to acquire images of the bubbles from below the boiling chamber using a high-speed camera (Vision Research Phantom IV) set to acquire 256x256 resolution images. Side view images of the bubbles were obtained (256x256 resolution) using a second high-speed camera (Vision Research Phantom V). Through the system multiplexer, the high-speed cameras were synchronized to acquire an image during the same rising edge TTL pulse from the computer. Two banks of high performance LED's provided the light for each camera view.

Imposed boundary condition. It should be noted that the boundary condition imposed on the bubble is not strictly constant wall heat flux because of the non-uniform substrate conduction across the heater array, and because 18 of the 96 heaters were non-functional (it is difficult to get all 96 heaters functioning when the line width is only 2 μm). The substrate conduction issue will be discussed in a future paper where it is accounted for. The non-functional heaters are difficult to account for, but the conclusions we will draw from the data do not seem to be affected by their presence.

RESULTS

The boiling rig utilized distilled and degassed FC-72 as the working fluid. The voltage at the top of the bridge was initially set to be a high value (V_{top} between 8.7 V to 10 V) for 3.5 s to initiate nucleation on the surface, after which the voltage was dropped to the set value (V_{top}) between 6.2 V to 8.3 V for 14.2 s. The bulk fluid temperature was 52.3 °C (+/- 0.2 °C) and the dissipative heat flux ($q''_{supplied}$) supplied to the array ranged from 14 to 25 W/cm^2.

Wall temperature variations. The spatially averaged temperature of the middle 64 heaters vs. time is shown on Figure 5 for four representative voltages. Frame 0 corresponds to when the voltage drops to the set value, with each subsequent frame obtained 0.000885s from the last (1130 Hz acquisition rate). All of the heater temperatures initially decay as a result of the drop in voltage, but then approach a steady value. Visual observation of the boiling behavior indicated that only a single bubble was observed on the surface when V_{top} was 6.8 V and lower. For the 6.2 V case, nucleation ceased altogether beginning from frame 1450, resulting in an increase in the wall temperature as the wall adjusts to the natural convection above the heater. Oscillations in the temperature are seen when bubbles are present on the surface. Multiple bubbles were observed to coexist on the surface when the voltage was 7.1 V and higher. For the 8.3 V case, multiple satellite bubbles surrounding a single large bubble and merging with it were observed. The bubble behavior for various voltage levels is discussed in detail below.

Temperature variations due to single bubbles. Single bubbles regularly departing one after another were observed for the 6.2 V, 6.5 V, and 6.8 V cases (dissipative heat fluxes of 14, 15, and 16 W/cm^2, respectively). Images (frames 825-859) of a bubble nucleation and departure event for the 6.8 V case are shown on Figure 6 where every other frame of the high-speed video is presented. Each of the heaters has been colored according to its temperature. Non-functional heaters are not colored. The dark rings that are clearly visible in the images result from shadows cast by the growing bubble. It can be shown from simply ray tracing (see Yin et al. [7]) that the outer diameter of this ring corresponds to the diameter of the bubble while the thickness of the ring depends on the bubble shape. A thin ring means the bubble shape is close to being hemispherical. Thicker rings result from a more spherical bubble. The inside diameter of the ring can also be a measure of the dry spot size.

Departure of a bubble is observed in Frames 825-831. The outer diameter of the ring remains roughly constant while the inner diameter decreases, indicating rewetting of the dry spot by liquid as the bubble pulls off the surface. Nucleation of a new bubble and its rapid growth are observed in Frames 833-839. The images show that the bubble grows hemispherically through Frame 841, as indicated by the thin, dark ring, to a maximum diameter of about 900 microns. The bubble takes about 7 ms to reach this size from nucleation–this is significantly slower than was observed for a similar bubble growing on a constant temperature surface for which it took less than 2 ms to reach its maximum size [6]. It is believed that a dry spot forms on the wall under the bubble during this time. The bubble then becomes progressively more spherical as indicated by the thickening of the ring, during which liquid rewets the surface. Bubble departure occurs at Frame 859 after which a new bubble immediately nucleates and grows.

The heater temperatures under the growing bubble do not decrease during initial hemispherical bubble growth (frames 833-839), implying that the energy for bubble growth could not have come from the wall, and must have come from the superheated liquid layer. The heaters under the bubble increase in temperature once a dry spot forms since power is continually supplied to them while little energy is removed by the low thermal conductivity vapor (frames 841-849). These same heaters are observed to decrease in temperature as they are rewet by liquid as the bubble departs the surface (frames 851-859).

The spatially averaged temperature of the middle 64 heaters vs. time over a small time scale are shown on Figure 7–the times at which the individual bubbles pinch off and depart the surface, and the times at which the bubble diameter reaches a maximum are indicated. During nucleation and growth of a bubble on the surface, the wall temperature

increases, while it decreases as the surface is rewet by liquid during bubble departure. Clearly, rewetting of the surface is associated with higher wall heat transfer. The bubble departure frequency is roughly 44 Hz for the three power levels shown.

Temperature variations due to bubble coalescence. Multiple bubble coalescence was observed at 7.1 V (dissipative heat flux of 18 W/cm^2) and higher. Images of the bubble behavior along with the temperature distribution are shown on Figure 8 for 7.1 V. A bubble departure event occurs on Frame 672. Nucleation and growth of a new bubble occurs beginning on Frame 673 (not shown). The bubble reaches its maximum size on Frame 681 (not shown), then begins to depart. During this departure process, a new bubble nucleates under this departing bubble (Frame 684, lower right corner), grows, coalesces with the departing bubble (Frame 690), after which the coalesced bubble departs the surface. Nucleation and growth of three new bubbles then occurs beginning Frame 692. Two of these bubbles coalesce in Frame 696 while the third bubble continues to grow in the lower right. Coalescence of the third bubble with the previously coalesced bubble occurs beginning Frame 712. The maximum bubble size occurs in Frame 716, after which the bubble begins to depart the surface. Departure occurs at Frame 726.

The average heater temperature during this series of events is shown on Figure 9. Bubble pinch off, maximum bubble size, and coalescence events are noted. Coalescence events are seen to cause small drops in the heater temperature, but bubble departure is observed to cause the largest drops in wall temperature. Coalescence may become more significant at higher heat fluxes when bubble merger occurs more frequently. Bubble coalescence can also lead to earlier departure of bubbles due to the increased size of the coalesced bubbles, indirectly leading to higher wall heat transfer.

The bubble behavior for 8.3 V (dissipative heat flux of 25 W/cm^2) was very chaotic. Numerous bubbles could exist on the surface simultaneously, and these bubbles coalesced with each other as they grew. The coalesced bubble moved randomly on the heater as it coalesced with other satellite bubbles, eventually forming a single large bubble on the surface under which dryout occurred. Departure of the coalesced bubble occurred occasionally, but there was no precisely defined bubble pinch-off event. As the coalesced bubble rewet the surface during departure, the wall temperature was hot enough to cause nucleation within the liquid front as it rewet the surface. Bubble growing underneath the departing bubble and merging with it were observed. Fluctuations in average wall temperature through a few departure cycles are shown on Figure 10. Again, large drops in wall temperature are associated with departure of the coalesced bubble, and the maximums in temperature occur when the dry area is largest. The departure frequency of the coalesced bubble is much lower than that of individual bubbles.

Future work. While the temperature measurements discussed above are indicative of when large amounts of heat are transferred, it is difficult to quantify the amount of heat transfer since a large portion of the dissipative heat supplied to the heaters are conducted away through the substrate. Local heat flux distributions are currently being computed using a 3-D, transient conduction simulation. At the heater array location on the upper surface of the substrate, the experimentally measured temperature field is imposed as a temporally varying temperature boundary condition. The remaining part of the substrate upper surface is assumed to exhibit a constant heat transfer coefficient, estimated from the average heater/bulk fluid temperatures. Once completed, the simulation will yield the calculated substrate temperature field at each experimental acquisition time, from which the average conduction heat transfer of each heater into the substrate can be estimated. The heat flux from the wall into the bulk fluid will be obtained by subtracting the substrate conduction from the power supplied to the heaters.

CONCLUSIONS

Time and space resolved temperature measurements, correlated to high speed images of bubble nucleation, growth and release in FC-72, were obtained using a heater array consisting of 96 100 μm heaters operated with a constant heat flux. At moderate heat flux levels, it was observed during initial nucleation and growth of a single bubble that the heater surface temperature experiences a moderate increase, indicating that the superheated liquid layer is a substantial energy source in initial bubble growth. As a bubble dry spot forms over the heater, the temperature increases due to the low thermal conductivity of the vapor, before dropping significantly as the bubble departs and liquid rewets the surface, increasing the wall heat transfer rate. For larger dissipative heat fluxes, multiple bubble coalescence events were observed. Although some decrease in the average heater array temperature occurred during bubble coalescence, the most significant temperature drop resulted from bubble departure. The bubble acts to remove the superheated liquid layer and decrease the temperature of the liquid locally, enabling higher wall heat transfer.

REFERENCES

1. Mikic, B.B. and Rosenhow, W.M. (1969), "Bubble growth rates in non-uniform temperature field", Prog. in Heat and Mass Transfer, Vol. II, pp. 283-292.
2. Cooper, M.G. and Lloyd, A.J.P. (1969), "The microlayer in nucleate boiling", Int. J. of Heat and Mass Transfer, Vol. 12, pp. 895-913.
3. Stephan, P. and Hammer, J. (1995), "New Model for Nucleate Boiling Heat Transfer", Heat and Mass Transfer/Waerme-und Stoffuebertragung, Vol 30, No. 2, p 119-125.
4. Wayner,P.C., Kao, Y.K. and LaCroix, L.V. (1976), Int. J. Heat Mass Transfer, Vol. 19 (1976) 487.

5. Yaddanapudi, N., and Kim, J., "Single Bubble Heat Transfer in Saturated Pool Boiling of FC-72", Multiphase Science and Technology, Vol. 12, No. 3-4, pp. 47-63, 2001.
6. Demiray, F. and Kim, J., Heat Transfer from a Single Bubble Nucleation Site During Saturated Pool Boiling of FC-72 Using an Array of 100 Micron heaters. 8th AIAA/ASME Joint Thermophysics and Heat Transfer Conference, June 2002.
7. Yin, Z., Prosperetti, A, Kim, J. "Bubble Growth on an Impulsively Powered Microheater", International Journal of Heat and Mass Transfer, Vol. 47, No. 5, pp. 1053-1067, 2004.

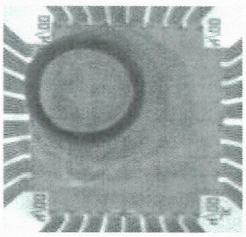

Figure 1: Photograph of heater array with single bubble nucleating on surface as seen from below the heater.

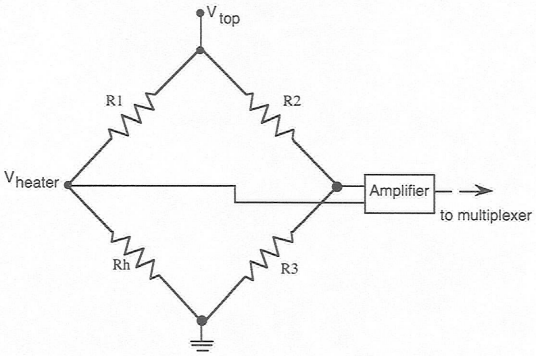

Figure 2: Circuit schematic for one heater.

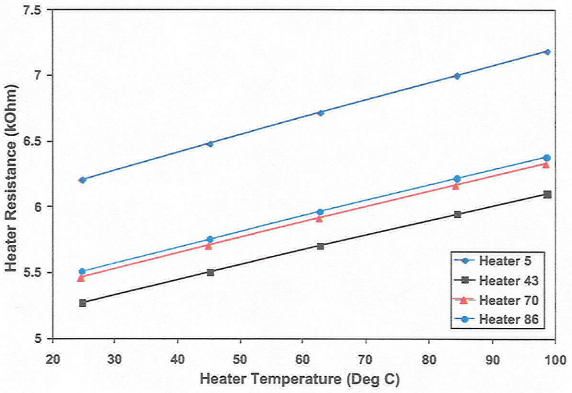

Figure 3: Plot of Heater resistance versus temperature calibration results for four selected heaters (one in each quadrant of the heater array).

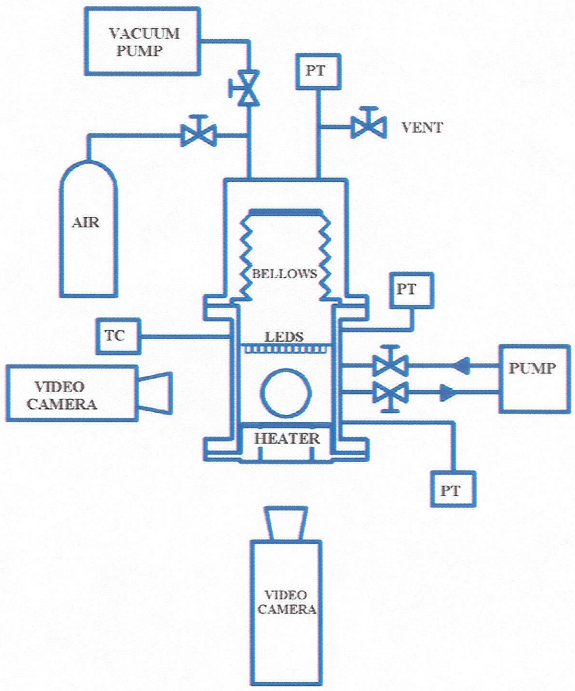

Figure 4: Illustration of custom designed boiling rig.

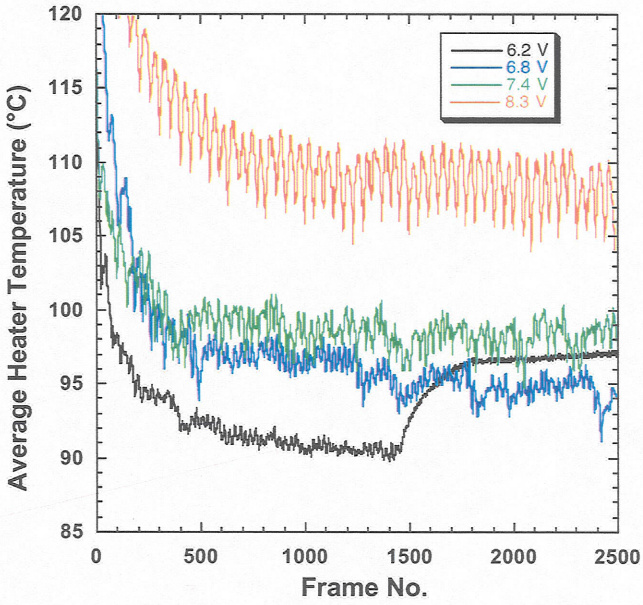

Figure 5: Average heater temperatures (middle 64 heaters) vs. time. Each frame represents 0.000885s.

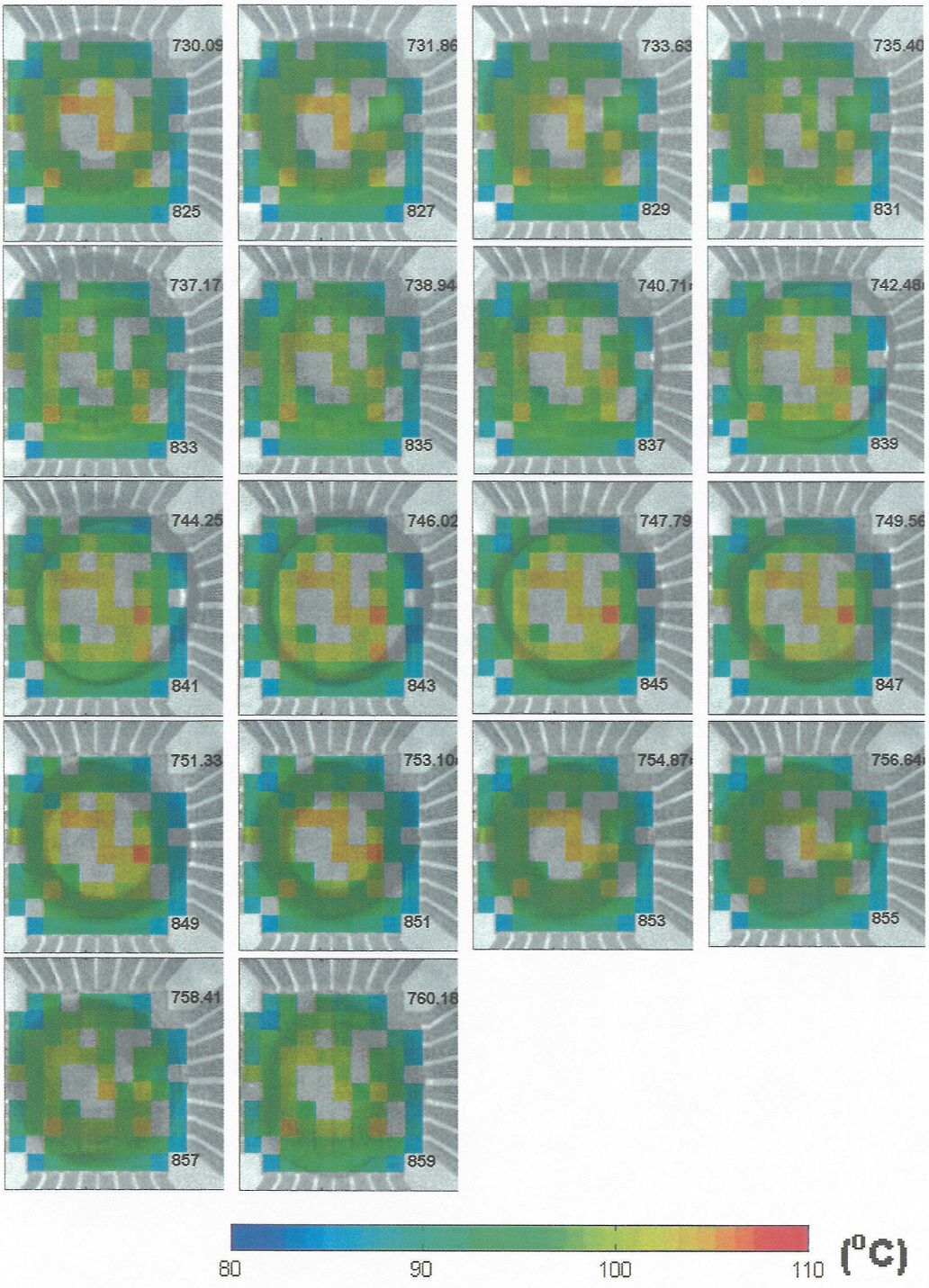

Figure 6: Surface temperature distribution through one bubble nucleation and departure cycle at 6.8 V. The time and frame numbers are given in the upper right and bottom right respectively of each frame.

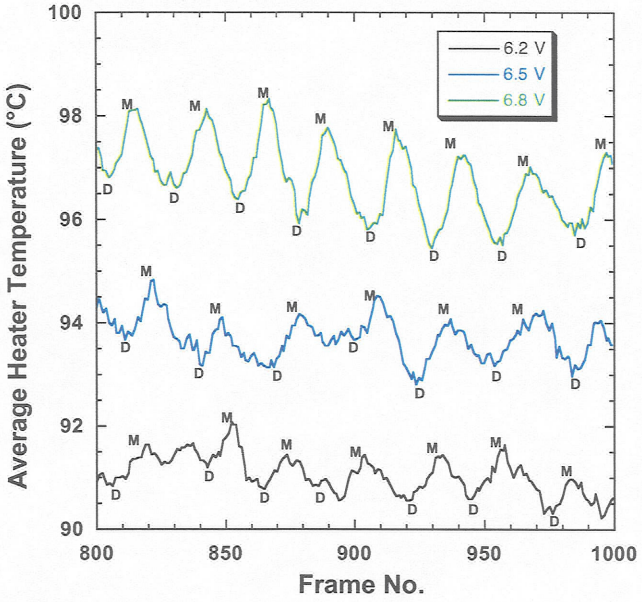

Figure 7: Temperature oscillations on the surface due to single bubble nucleation and departure (D=bubble departure, M=maximum diameter of bubble) at low voltages.

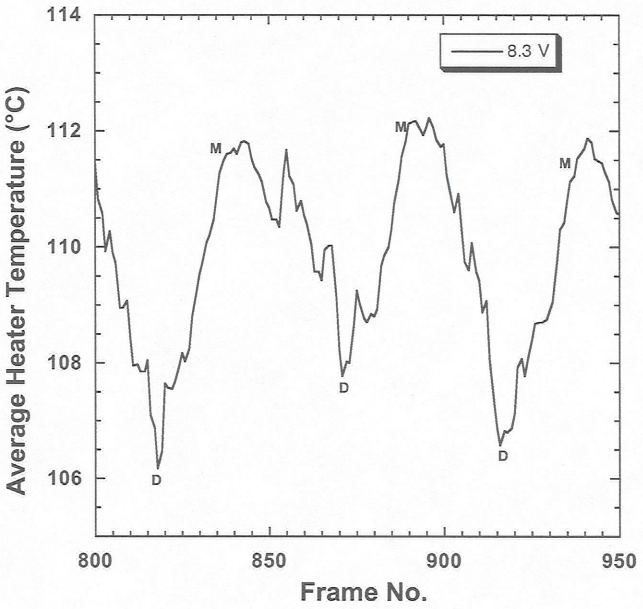

Figure 10: Heater temperature during bubble coalescence (D=bubble departure, M=maximum diameter of bubble), 8.3 V.

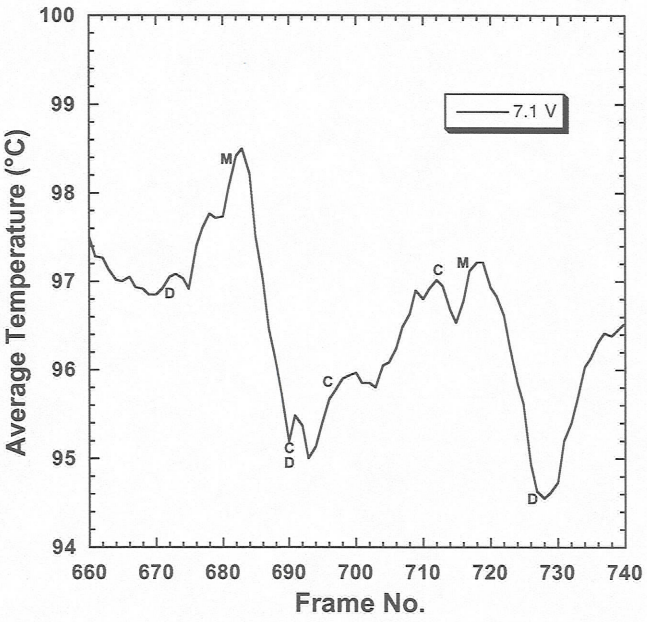

Figure 9: Heater temperature during bubble coalescence (D=bubble departure, M=maximum diameter of bubble, C=bubble coalescence), 7.1 V.

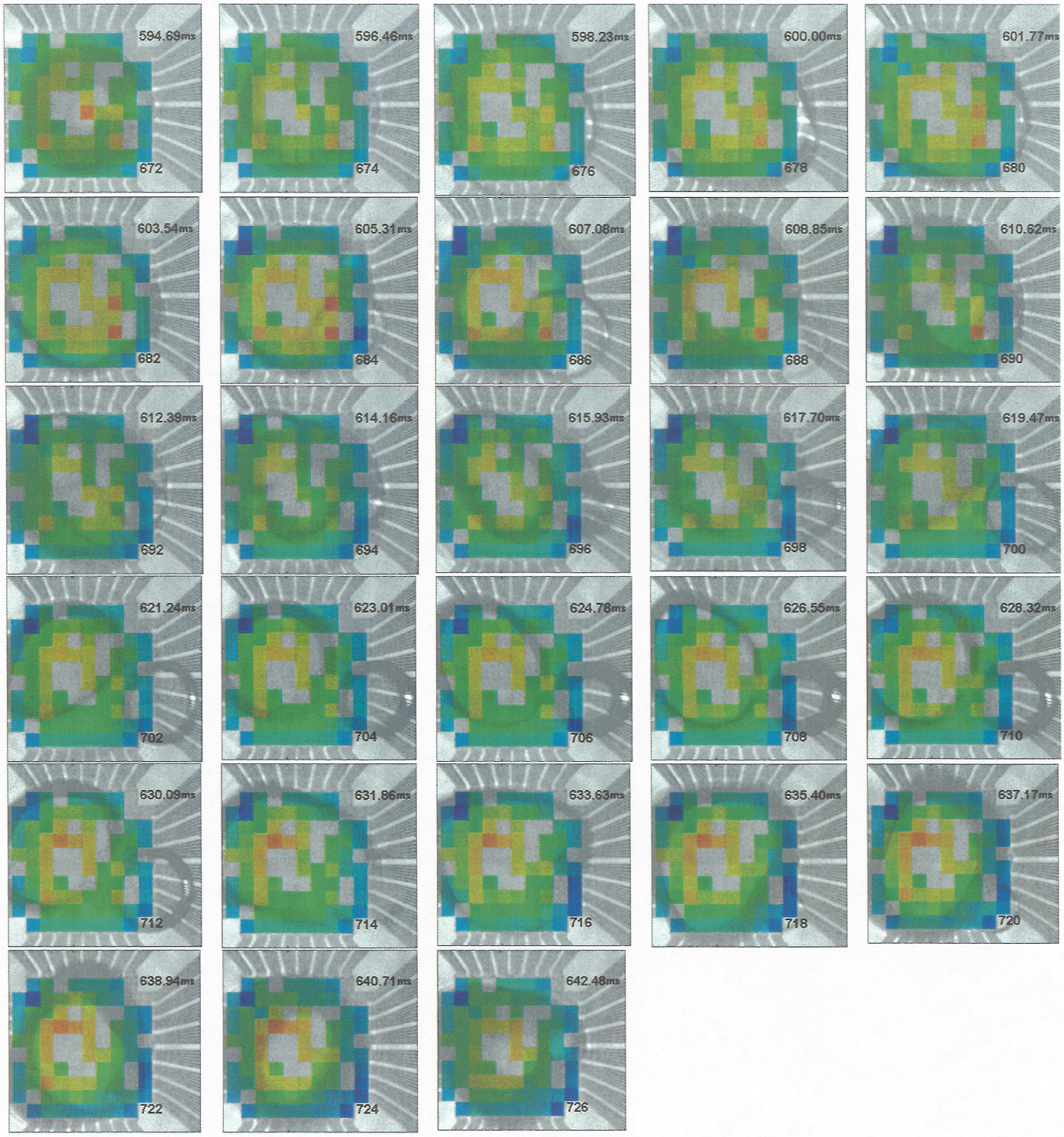

Figure 8: Surface temperature distribution through a bubble coalescence event at 7.1 V. The time and frame numbers are given in the upper right and bottom right respectively of each frame. The temperature scale is the same as shown on Figure 6.